IOP Publishing Physica Scripta
Phys. Scr. 95 (2020) 105601 (10pp) https://doi.org/10.1088/1402-4896/abb2e0

A new class of Ion-acoustic solitons that can exist below critical Mach number

G S Lakhina[1,3], S V Singh[1] and R Rubia[2]

[1] Indian Institute of Geomagnetism, Plot No. 5, Sector- 18, New Panvel (W), Navi Mumbai-410218, India
[2] P-12/14 Tarapore Enclave, Rangpuri, New Delhi-110070, India

E-mail: gslakhina@gmail.com, satyavir@iigs.iigm.res.in and rubi.r92@gmail.com

Received 10 July 2020, revised 18 August 2020
Accepted for publication 26 August 2020
Published 3 September 2020

Abstract

It is commonly believed that ion-acoustic solitons can only exist above the critical Mach number in a plasma system. A new class of ion-acoustic solitons that can exist below the critical Mach number is reported for the first time in a three-component plasma consisting of hot Maxwellian electrons, and two counterstreaming ion beams. The analysis is based on the Sagdeev pseudopotential technique, and considers a simple case of two counterstreaming proton beams with equal density and streaming velocity. Linear stability analysis shows that the slow ion-acoustic modes become unstable due to ion beam instability when the beam velocity normalized with the ion acoustic speed, U_0, is in the range of $0.55 \leqslant U_0 \leqslant 1.14$. It is shown that when the normalized streaming velocity is below or at a threshold value, $U_{th} = 1.14$, only the regular solitons having Mach numbers greater than critical Mach number can exist. However, when the streaming velocity exceeds the threshold value (all modes are stable), both regular and the new class of ion-acoustic solitons can exist. A special case of unequal ion densities and unequal streaming velocities of the counterstreaming beams is considered in appendix, and similar effects are found. Hence, the new class of slow ion-acoustic solitons can exist in the parametric regime where the system is stable to counterstreaming ion beams instability. The results could be useful in the interpretation of slow electrostatic solitary waves (ESWs) observed in the magnetosphere.

Keywords: slow ion-acoustic solitons, electrostatic solitary waves, nonlinear ion-acoustic waves, multi-ion plasma system

(Some figures may appear in colour only in the online journal)

1. Introduction

Sagdeev [1] and Washimi and Taniuti [2] were the first to investigate ion-acoustic solitons in plasmas. A great interest in the theoretical studies of ion-acoustic solitons and double layers [3–31] was generated by the observations of electrostatic solitary waves (ESWs) in the Earth's magnetosphere by several spacecrafts, like S3-3 [32], Viking [33, 34], Geotail [35], Polar [36–39] and FAST [40, 41], Cluster [42], Wind [43], etc. In these studies, ion-acoustic solitons and double layers were investigated in multi-component unmagnetized as well as magnetized plasmas, and various plasma species were treated either as fluids or having Maxwellian particle distributions. There are several studies dealing with the ion-acoustic solitary waves with highly energetic kappa-distributed electrons or nonthermal electrons with Cairns type distributions [44–52].

The general features of the ion-acoustic solitons, from the above studies, are: (i) the solitons exist when the Mach number, M, is greater than the critical Mach number, M_0, and (ii) the soliton amplitude increase with increase of M till maximum Mach number, $M_{\max}$, is reached, and no ion-acoustic solitons can exist beyond it, (iii) under certain conditions ion-acoustic solitons go over to the double layer at $M = M_{DL} = M_{\max}$. (iv) In multi-species (three or more) plasma, and under specific conditions,'super solitons' with Mach number greater than M_{DL} can exist [23, 28, 53–58].

Several laboratory experiments [3, 59–63] and simulation studies [64–69] on ion-acoustic solitons confirm the above findings based on fluid theories.

[3] Author to whom any correspondence should be addressed.

It is important to point out that near M_{max} ion-reflection may occur at the ion-acoustic solitons turning them into the ion-acoustic shocks [1, 70]. Interestingly the existence domain of such ion-acoustic shock extends beyond M_{max} of ion-acoustic solitons. However, the ion reflection at the soliton is a kinetic process, and thus, it cannot be studied by the fluid theory used here. One must employ the kinetic theory to study ion-reflection at the soliton [70]. Since the focus of study is not the ion-acoustic shocks due to ion reflection which occur near M_{max}, but rather the new class of slow ion-acoustic solitons which can exist below critical Mach number M_0, the ion-reflection is not expected to be important and, therefore, the use of fluid theory is justified.

Here, we discuss a new class of ion-acoustic solitons which are supported by multispecies plasma containing ion beams. These solitons exist in the the Mach number range of $M_{min} < M < M_0$, i.e, below the critical Mach number, M_0, but above a certain minimum Mach number, M_{min}. The amplitudes of these solitons increase with decrease of the Mach number till M_{min}, and no solitons can exist below it.

Summary: For the first time, existence of a new class of ion acoustic solitons below critical Mach number is shown in three-component plasma composed of hot Maxwellian electrons and two counterstreaming ion beams. Linear stability analysis shows that the slow ion-acoustic modes become unstable due to ion beam instability in a certain range of beam velocities for the plasma parameters considered. Two special cases: 1. Equal ion beam densities and equal velocities of the counterstreaming ion beams, and 2. Unequal ion densities and unequal velocities of the counterstreaming ion beams are considered. For both the cases, the new class of slow ion-acoustic solitons can occur only when the system becomes stable against the ion beam instability. Though existence of new class of slow ion-acoustic solitons is shown for two special cases only, they can occur over a wide range of ion beam densities, temperatures, and streaming velocities of the counterstreaming ion beams.

A theoretical model for ion-acoustic solitons is presented in the next section, whereas a special case of counter-streaming proton beams is given in section 3. The results are summarized in section 4.

2. Model for ion-acoustic solitons

We consider a three-component magnetized plasma consisting of hot Maxwellian electrons with density, N_e and temperature, T_e, and two fluid proton beams with densities N_1 and N_2, temperatures T_1 and T_2, and beam speeds along the ambient magnetic field, $\mathbf{B}_0 = B_0\mathbf{x}$, as V_1 and V_2, respectively. Here, subscripts 1 and 2 refer to the parameter of proton beam 1 and proton beam 2, respectively. To maintain charge neutrality in the equilibrium state, we take $N_e = N_1 + N_2$. We consider the electrostatic waves propagating parallel to the magnetic field $\mathbf{B}_0$.

Since the hot electrons follow the Maxwellian distribution, their normalized number density in the presence of ion-acoustic waves with potential ϕ can be written as [30]

$$n_e = \exp(\phi) \tag{1}$$

The dynamics of proton beams is governed by following fluid equations [71]:

$$\frac{\partial n_j}{\partial t} + \frac{\partial (n_j v_j)}{\partial x} = 0 \tag{2}$$

$$\frac{\partial v_j}{\partial t} + v_j \frac{\partial v_j}{\partial x} + \frac{1}{n_j}\frac{\partial P_j}{\partial x} + \frac{\partial \phi}{\partial x} = 0 \tag{3}$$

$$\frac{\partial P_j}{\partial t} + v_j \frac{\partial P_j}{\partial x} + 3P_j \frac{\partial v_j}{\partial x} = 0 \tag{4}$$

where $j = 1$ and 2 for the proton beams 1 and 2, respectively, and the adiabatic index $\gamma_j = 3$. Here, the number densities are normalized by the equilibrium number density of electrons, $N_0 = N_e = N_1 + N_2$, velocities are normalized with the ion-acoustic speed, $C_a = \sqrt{T_e/m_p}$; m_p is the mass of the proton, lengths are normalized with the electron Debye length, $\lambda_{de} = \sqrt{T_e/4\pi N_0 e^2}$; e is the electronic charge, time is normalized with the inverse of the proton plasma frequency, $\omega_{pp} = \sqrt{4\pi N_0 e^2/m_p}$ and electrostatic potential, ϕ is normalized with T_e/e, and the thermal pressure P_j with $N_e T_e$. Similarly, $\sigma_j = T_j/T_e$, $n_j^0 = N_j/N_0$ and $U_j = V_j/C_a$ are the normalized temperature, equilibrium number density, and drift speed of the jth species.

The above basic set of equations is closed by the Poisson's equation:

$$\frac{\partial^2 \phi}{\partial x^2} = (n_e - n_1 - n_2) \tag{5}$$

2.1. Linear stability

Before doing the nonlinear analysis for the ion-acoustic waves, we shall investigate the linear stability of the system briefly. The linear dispersion relation can be derived by linearizing equations (1)–(5) and it can be written in unnormalized form as:

$$1 + \frac{1}{k^2\lambda_{de}^2} = \frac{\omega_{p1}^2}{(\omega - kV_1)^2 - 3k^2 v_{t1}^2} + \frac{\omega_{p2}^2}{(\omega - kV_2)^2 - 3k^2 v_{t2}^2} \tag{6}$$

where $\omega_{p1,2} = \sqrt{4\pi N_{1,2} e^2/m_p}$, $v_{t1,2} = \sqrt{T_{1,2}/m_p}$. In general, equation (6) is a 4th order in ω and has four roots corresponding to two fast ion-acoustic (having higher frequencies and phase velocities) and two slow ion-acoustic modes (with smaller frequencies and phase velocities). However, for the special case of $V_1 = V_2 = 0$ and $v_{t1} = v_{t2} = v_t$, it becomes quadratic in ω and has the solution:

$$\omega^2 = \frac{k^2 C_a^2}{1 + k^2\lambda_{de}^2} + 3k^2 v_t^2 \tag{7}$$

which represents two fast ion-acoustic waves, one with $\omega > 0$ propagates along x and the other with $\omega < 0$ propagates along -x direction. For $v_{t1} \neq v_{t2}$, equation (6) has the following solution,

$$\omega_{\pm}^{2} = \frac{1}{2}[B \pm \sqrt{B^{2} - 4C}]$$

$$\text{where} \quad B = \frac{k^{2}C_{a}^{2}}{1 + k^{2}\lambda_{de}^{2}} + 3k^{2}v_{t1}^{2} + 3k^{2}v_{t2}^{2}$$

$$\text{and} \quad C = \frac{3k^{2}c_{s}^{2}}{1 + k^{2}\lambda_{de}^{2}} \frac{(k^{2}v_{t2}^{2}\omega_{p1}^{2} + k^{2}v_{t1}^{2}\omega_{p2}^{2})}{\omega_{pp}^{2}} + 9k^{4}v_{t1}^{2}v_{t2}^{2} \tag{8}$$

The $\pm$ sign corresponds to fast and slow ion acoustic modes [30]. In the limit of $k^2\lambda_{de}^2 \ll 1$, above equation (8) reduces to that derived by Mahmood and Ur-Rehman(2013) [29] and Ur-Rehman *et al* (2014) [31] for the case of ions having equal masses and for adiabatic index $\gamma = 3$. It is to be noted that equation (17) of Sreeraj *et al* (2016) [72] reduces to the above equation for $\gamma = 3$, Maxwellian electrons ($\kappa \to \infty$) and two protons having different temperatures.

The dispersion relation (6) can be studied numerically, and it is found that for a given set of plasma parameters, the system becomes unstable for a certain range of ion beam velocities. In figures 1(a)–(d), we have shown variation of normalized frequency ω/ω_{pp} with normalized wave number, $k\lambda_{de}$, obtained from the solution of equation (6) for the counterstreaming ion beams moving with equal and opposite velocity, U_0, and having equal density and temperature. The curves 1 and 4 are for the fast ion acoustic modes and the curves labeled as 2 and 3 are for the slow ion-acoustic modes. For $U_0 = 0.0$ (see panel a of figure 1), it is seen that fast ion-acoustic modes (cf curves 1 and 4) have real roots. The curve 1 is for the fast ion-acoustic mode having $\omega_r > 0$ (positive phase velocity), and it is propagating along B_0. The curve 4 is for the fast ion-acoustic mode having $\omega_r < 0$ (negative phase velocity) and it propagates anti-parallel to B_0. Note that ω_r for curves 1 and 4 have equal and opposite values due to symmetry in the system. The slow ion-acoustic modes do not exist in this case. Therefore, the system is stable. From panel b of figure 1, it is noticed that for $U_0 = 0.5$, the system is stable as the fast ion-acoustic modes (curves 1 and 4) as well as slow ion-acoustic modes have real roots. One fast ion-acoustic mode (curve 1) and one slow ion-acoustic mode (curve 2) propagate along B_0, and the other fast mode (curve 4) and slow ion-acoustic mode (curve 3) propagate anti-parallel to B_0. For $U_0 = 1.0$ (see panel c of figure 1), it is seen that the fast ion-acoustic modes (curves 1 and 4) have real roots whereas the slow ion-acoustic modes have purely imaginary roots (see solid curves 2 and 3) for $0 < k\lambda_{de} < 0.6$. The solid curve 2 has positive values corresponding to the growing mode. The solid curve 3 has negative values and is a damped mode. For $k\lambda_{de} > 0.6$, these roots have real values, as seen from the dashed curves 2 and 3, and the system becomes stable. For $U_0 = 1.5$ (see panel d of figure 1), all the roots are real and the system is stable. For this system, our numerical computations show that the ion beam instability occur for $0.55 \leqslant U_0 \leqslant 1.14$ (not shown).

It should be noted that due to the symmetry in the system for this special case, the real frequencies of the parallel and anti-parallel propagating modes are equal and opposite for both fast and slow ion-acoustic modes. For unequal beam densities or beam velocities, the parallel and anti-parallel modes would have different ω_r and phase velocities as discussed in the appendix. Although not shown in the appendix, having unequal ion-beam temperatures can also introduce asymmetry in the system, and can produce unequal phase velocities of parallel and anti-parallel propagating ion-acoustic modes.

2.2. Nonlinear analysis

In order to study the properties of ion-acoustic solitons, the set of equations (2)–(5) is transformed into a stationary frame moving with phase velocity, V of the electrostatic solitary wave, i.e., $\xi = (x - Mt)$, where $M = V/C_a$ is the Mach number. In such a reference frame, all variables, e.g., densities, fluid velocities and pressure tend to their undisturbed values, and the electrostatic potential $\phi = 0$, and $d\phi/d\xi = 0$ at $\xi \to \pm\infty$. Then, from equations (2)–(4) we can get the following expressions for the densities of the proton beams [15, 18, 30]:

$$n_1 = \frac{n_1^0}{2\sqrt{3\sigma_1}}\{[(M - U_1 + \sqrt{3\sigma_1})^2 - 2\phi]^{1/2} - [(M - U_1 - \sqrt{3\sigma_1})^2 - 2\phi]^{1/2}\} \tag{9}$$

$$n_2 = \frac{n_2^0}{2\sqrt{3\sigma_2}}\{[(M - U_2 + \sqrt{3\sigma_2})^2 - 2\phi]^{1/2} - [(M - U_2 - \sqrt{3\sigma_2})^2 - 2\phi]^{1/2}\} \tag{10}$$

On substituting n_e, n_1 and n_2 in the transformed Poisson's equation (5), multiplying it with $d\phi/d\xi$ and integrating with the boundary conditions that $\phi = 0$, $d\phi/d\xi = 0$ at $\xi \to \pm\infty$, we get the energy integral [18, 30, 71]

$$\frac{1}{2}\left(\frac{d\phi}{d\xi}\right)^2 + S(\phi, M) = 0 \tag{11}$$

The above equation (11) describes the motion of a pseudo-particle of unit mass in a pseudopotential $S(\phi, M)$, where, ϕ and ξ play the role of displacement from the equilibrium and time, respectively. The Sagdeev pseudopotential, $S(\phi, M)$, is given by [30, 51, 52, 71]

$$\begin{aligned} S(\phi, M) = {} & [1 - \exp\phi] \\ & + \frac{n_1^0}{6\sqrt{3\sigma_1}}\{(M - U_1 + \sqrt{3\sigma_1})^3 \\ & - [(M - U_1 + \sqrt{3\sigma_1})^2 - 2\phi]^{3/2} \\ & - (M - U_1 - \sqrt{3\sigma_1})^3 \\ & + [(M - U_1 - \sqrt{3\sigma_1})^2 - 2\phi]^{3/2}\} \\ & + \frac{n_2^0}{6\sqrt{3\sigma_2}}\{(M - U_2 + \sqrt{3\sigma_2})^3 \\ & - [(M - U_2 + \sqrt{3\sigma_2})^2 - 2\phi]^{3/2} \\ & - (M - U_2 - \sqrt{3\sigma_2})^3 \\ & + [(M - U_2 - \sqrt{3\sigma_2})^2 - 2\phi]^{3/2}\} \end{aligned} \tag{12}$$

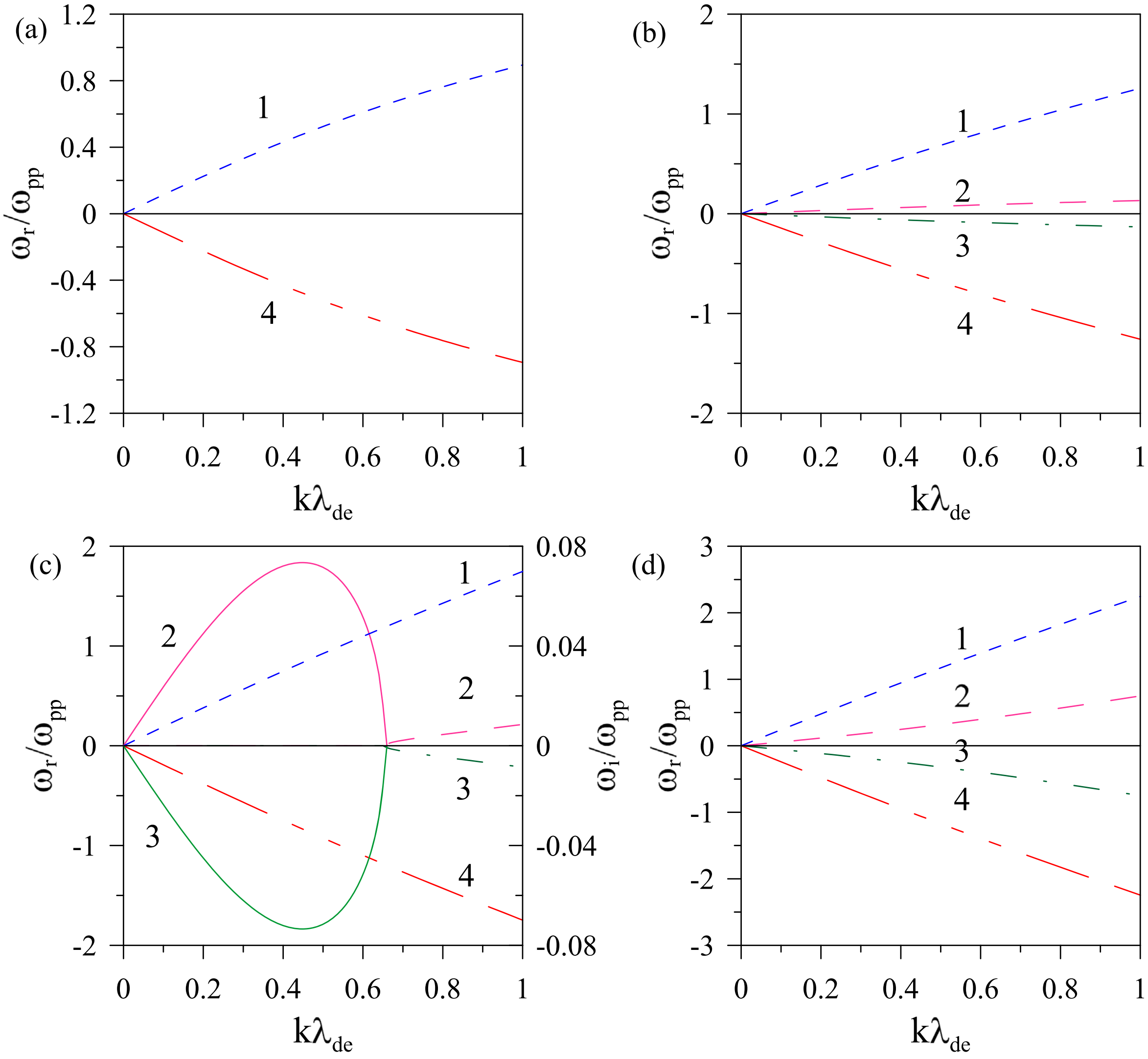

Figure 1. Dispersion relation for the ion-acoustic waves showing the frequency ω/ω_{pp} versus wave number, $k\lambda_{de}$ for the counterstreaming ion beam case for the normalized parameters: $n_1^0 = n_2^0 = 0.5$, $\sigma_1 = \sigma_2 = \sigma_p = 0.1$. In Panels (a) to (d), the curves 1 and 4 correspond to fast ion-acoustic modes and the curves 2 and 3 correspond to the slow ion-acoustic modes. The broken curves are for the real frequency, ω_r/ω_{pp}, and they follow the scale on left side of the panel. The solid curves are for the imaginary frequency, ω_i/ω_{pp}, and they follow the scale given on the right side of the panel. The positive or negative values of ω_i/ω_{pp} represent, respectively, the growth rate or the damping rate of the mode. Panel (a) is for the case of $U_0 = 0.0$; slow ion-acoustic modes do not exist, and the roots corresponding to fast ion-acoustic modes (cf curves 1 and 4) have real values, thereby showing that the system is stable as expected. Panel (b) is for $U_0 = 0.5$, and it also shows that the system is stable as all roots are real. Panel (c) is for $U_0 = 1.0$, and here the fast ion-acoustic modes have real values (cf curves 1 and 4) whereas the slow ion-acoustic mode 2 is unstable and slow mode 3 is damped for $0 < k\lambda_{de} < 0.6$ (cf solid curves 2 and 3). For $k\lambda_{de} > 0.6$, slow ion-acoustic modes have real frequencies (cf broken curves 2 and 3). Panel (d) is for $U_0 = 1.5$, and all roots are real showing that the system is stable.

Please note that equation (12) is written in symbolic form where the operation of a square root on a squared expression returns the same expression, e.g., $\sqrt{(M \pm \sigma_j)^2} = (M \pm \sigma_j)$. Please note that in the absence of drift speed of proton beams, i.e., $U_1 = U_2 = 0$, the results of Lakhina *et al* (2014) [30] and Rubia *et al* (2016)[49] (in the limit $\kappa \to \infty$) can be obtained.

For the existence of soliton solutions, the Sagdeev pseudopotential $S(\phi, M)$ must satisfy the following conditions: (i) $S(\phi, M) = 0$, $dS(\phi, M)/d\phi = 0$, and $d^2S(\phi, M)/d\phi^2 < 0$ at $\phi = 0$, (ii) $S(\phi, M) = 0$ at $\phi = \phi_0$ (ϕ_0 is the amplitude of the soliton), and (iii) $S(\phi, M) < 0$ for $0 < |\phi| < |\phi_0|$.

The Sagdeev pseudopotential, S (ϕ, M) given by equation (12) and its first derivative with respect to ϕ vanish at $\phi = 0$. Defining $F(M) = d^2S(\phi, M)/d\phi^2$ at $\phi = 0$, we have

$$F(M) = \frac{n_1^0}{[(M - U_1)^2 - 3\sigma_1]} + \frac{n_2^0}{[(M - U_2)^2 - 3\sigma_2]} - 1 \qquad (13)$$

The soliton condition demands that $F(M) < 0$ must be satisfied. The critical Mach numbers, M_0 are the solution of $F(M_0) = 0$. So far the ion-acoustic soliton cases discussed in the literature correspond to the situations where for $M > M_0$, the condition $F(M) < 0$ is satisfied. These solutions are the familiar ion-acoustic solitons whose Mach numbers are larger than the critical Mach number M_0. Here, we will show that the soliton condition $F(M) < 0$, under certain plasma parameters in the presence of counterstreaming ion beams, can be satisfied for $M < M_0$. This corresponds to a new class of ion-acoustic solitons that can exist below the critical Mach number M_0.

3. Special case of counterstreaming proton beams

To illustrate, we consider a special case of equal density counterstreaming proton beams where $n_1^0 = n_2^0 = 0.5$, $T_1 = T_2 = T_p$ (i.e, $\sigma_1 = \sigma_2 = \sigma_p$), $U_1 = -U_0$ and $U_2 = U_0$. For this special case, both the charge and current neutrality is maintained in the equilibrium state. The critical Mach number, M_0 is obtained by solving $F(M_0) = 0$ from equation (13) either analytically or numerically. In the presence of beams, there are four possible roots for M_0, but all roots may not be physical.

For $U_0 = 0$, we get the critical Mach number $M_0 = \pm(1 + 3\sigma_p)^{1/2}$. In what follows, we shall consider the positive root only as the soliton associated with the negative root has the same properties except that it propagates in the opposite direction.

Figure 2 shows the variation of the Sagdeev potential $S(\phi, M)$ *versus* the normalized electrostatic potential ϕ for various values of the Mach number for the ion-acoustic solitons. In panel (a) the proton beam speed is $U_0 = 0.0$. The critical Mach number in this case occur at $M_0 = \pm 1.14$. The solitons occur for $M > M_0$. A look at the curves 1–4 shows that the ion-acoustic soliton amplitude increases with M from 1.2, 1.25 and 1.3 (cf. curves 1, 2, and 3). For the curve 4 for $M = 1.31$ and beyond, the solitons do not exist. Thus, these solitons occur in the Mach number range $M_0 < M < M_{max}$. In panel (b), the proton beam speed is $U_0 = 1.0$, and here two real critical Mach numbers occur at $M_0 = \pm 1.91$. The ion-acoustic soliton amplitudes increase with M from 1.96, 1.98 and 2.0 (cf curve 1, 2 and 3) and solitons do not exist for $M = 2.03$ (cf curve 4) and beyond. In panels (c) and (d), the protons beam speed is $U_0 = 1.5$. Here there are four real roots for critical Mach numbers at $M_0 = \pm 0.566$ and $\pm$ 2.41. The smaller critical Mach numbers corresponds to the slow ion-acoustic mode and the larger ones to the fast ion-acoustic mode [15, 30, 48, 71]. Panel (c) shows the results for the fast ion-acoustic solitons. Here also, the soliton amplitude increases with M from 2.48, 2.5 and 2.51 (cf curves 1,2 and 3), and for $M = 2.52$ (curve 4) and beyond, the fast ion-acoustic solitons do not exist. In panel (d), the results for the new class of slow ion-acoustic solitons are shown. In contrast to the cases shown in Panels (a), (b) and (c) where solitons occur for $M > M_0$, this new class of slow ion-acoustic solitons occur for $M < M_0$. Further, their amplitude increases as M decreases from 0.52, 0.5 and 0.45 (cf curves 1, 2 and 3, and for $M = 0.43$ (cf curve 4) and lesser values, the slow ion-acoustic solitons do not exist. Therefore, these solitons occur in the Mach number range $M_0 > M > M_{min}$. This behavior is opposite to that of the regular (both fast and slow) ion-acoustic solitons discussed in the literature [15, 30, 71] and also shown in panels (a), (b) and (c).

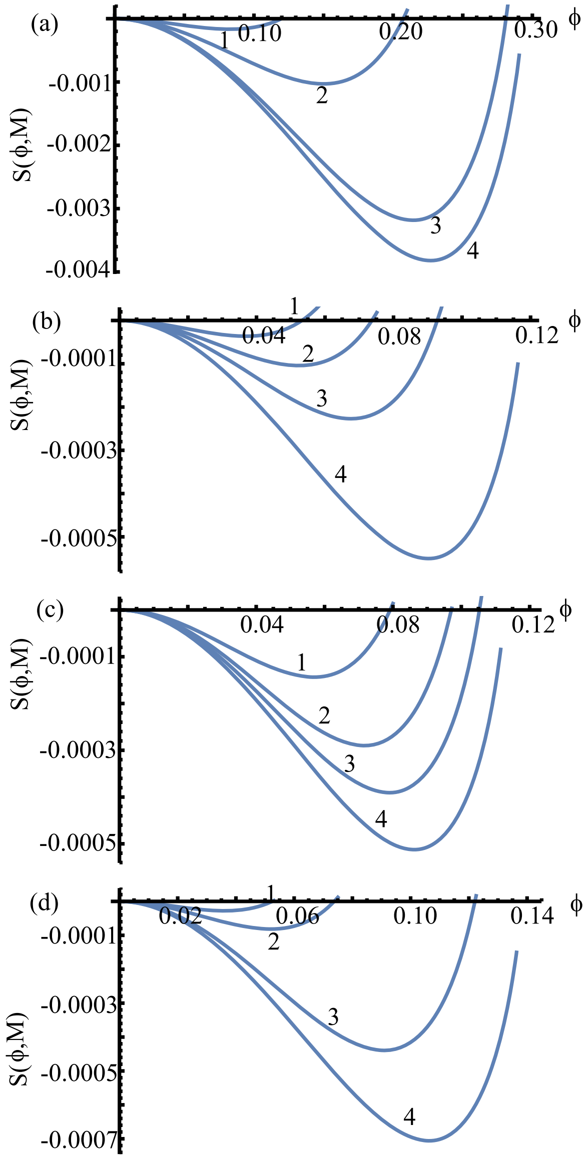

Figure 2. Sagdeev pseudopotential $S(\phi, M)$ *versus* the potential ϕ for the ion-acoustic solitons for the normalized parameters: $n_1^0 = n_2^0 = 0.5$, $\sigma_1 = \sigma_2 = \sigma_p = 0.1$. Panel (a), ion-acoustic solitons for the case of $U_0 = 0.0$, and $M = 1.2$, 1.25, 1.3, and 1.31 for the curves 1, 2, 3 and 4, respectively. Panel (b), fast ion-acoustic solitons for $U_0 = 1.0$, and $M = 1.96$, 1.98, 2.0 and 2.03 for the curves 1, 2, 3 and 4, respectively. Slow ion-acoustic solitons do not exist. Panel (c) fast ion-acoustic solitons for $U_0 = 1.5$, and $M = 2.48$, 2.5, 2.51, and 2.52 for the curves 1, 2, 3 and 4, respectively. Panel (d) slow ion-acoustic solitons for $U_0 = 1.5$, and $M = 0.52$, 0.5, 0.45, and 0.43 for the curves 1, 2, 3 and 4, respectively. These are new class of ion-acoustic solitons that occur below the critical Mach number.

To make sure that the new class of slow ion-acoustic solitons satisfy the soliton condition, in figure 3, we have shown the variation of $F(M)$ versus M for proton beam speeds of $U_0 = 0.0$ (panel (a)), 1.0 (panel (b)) and 1.5 (panel (c)) for the same plasma parameters as in figure 1. It is clear that

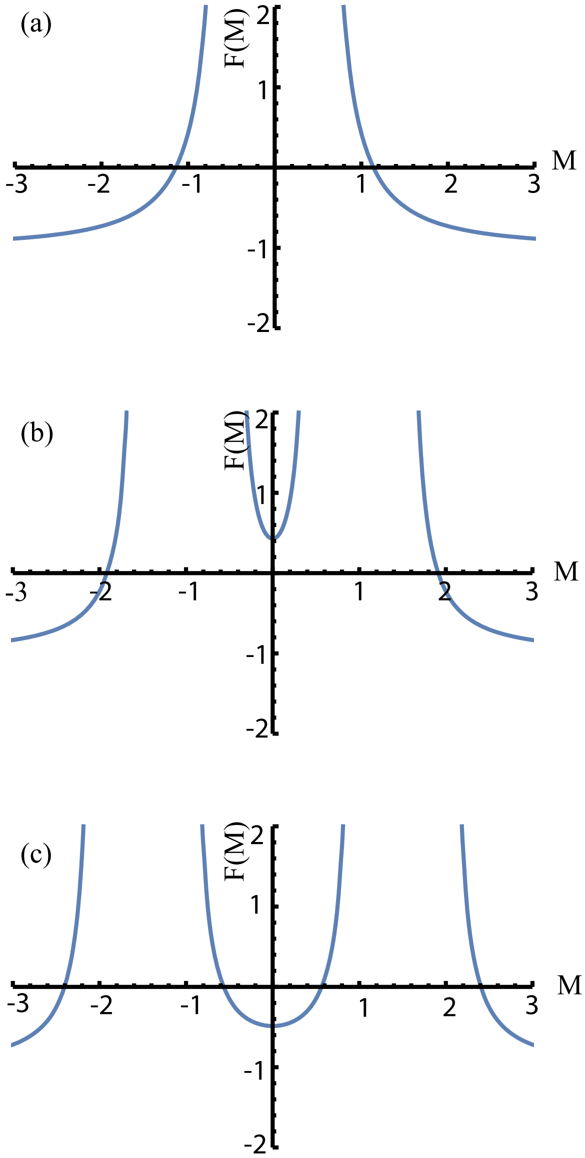

Figure 3. Variation of $F(M)$, the second derivative of the Sagdeev pseudopotential $S(\phi, M)$ at $\phi = 0$, *versus* the Mach number M for the normalized parameters: $n_1^0 = n_2^0 = 0.5$, $\sigma_1 = \sigma_2 = \sigma_p = 0.1$. Panel (a), $U_0 = 0.0$, and critical Mach numbers occur at $M_0 = \pm 1.1402$. Panel (b), $U_0 = 1.0$, only two critical Mach numbers (fast ion-acoustic) are real occurring at $M_0 = \pm 1.9124$, the other two roots are complex. Panel (c), $U_0 = 1.5$, and there are four real critical Mach numbers occurring at $M_0 = \pm 2.404$ (fast ion-acoustic) and $\pm$ 0.566 (slow ion-acoustic).

critical Mach number occurs at the places where the $F(M)$ curve cut the M axis. In panel (a), the critical mach numbers occur at $M_0 = \pm 1.14$, and for $M > M_0$, the $F(M)$ curves go below the M-axis, i.e., $F(M) < 0$, thus the soliton condition is satisfied. In panel (b) for $U_0 = 1.0$, there are two real critical Mach numbers at $M_0 = \pm 1.91$ (fast ion acoustic modes), and two complex roots which correspond to slow ion-acoustic modes. One of the slow ion-acoustic mode is growing while the other is a damped mode. The instability of slow ion-acoustic mode arises due to the counterstreaming ion beams, and it occurs at long wavelengths [73] as the linear analysis shows. Unfortunately, the Sagdeev pseudopotential technique used here deals with the time stationary solutions of the fluid equations and cannot handle the unstable or damped modes. The unstable mode can produce ion-acoustic turbulence which may affect the properties of the ion-acosutic soliton. However, there is an experimental evidence that coherent ion-acoustic solitons can coexist with the ion-acoustic turbulence [63]. Now, coming back to the real roots corresponding to fast ion-acoustic modes, it is observed from figure 3 (panel b) that the $F(M)$ curves go below the M-axis when M exceeds M_0, and the condition $F(M) < 0$ is satisfied. In panel (c), there are four real critical Mach numbers at $M_0 = \pm 0.566$ (slow ion-acoustic) and $\pm$ 2.41 (fast ion-acoustic). There are no unstable modes in conformity with the the linear analysis. It is clear that for the fast ion-acoustic modes, $F(M) < 0$ for $M > 2.41$, whereas for slow ion-acoustic modes, the condition $F(M) < 0$ is satisfied for $M < 0.566$. Hence, the slow ion-acoustic solitons are physical as they satisfy all the soliton conditions.

We would like to point out that due to the symmetry in the system for this special case, the real critical Mach number are equal and opposite for both fast and slow ion-acoustic solitons. In general, for the case of unequal beam densities or unequal beam velocities, the real critical Mach numbers for both fast and slow ion-acoustic solitons would have different values (in magnitude and sign). In appendix, one such special case is discussed where the normalized parameters are: $\sigma_1 = \sigma_2 = \sigma_p = 0.1$, $n_1^0 = 0.7$, $n_2^0 = 0.3$, $U_1 = -1.0$, and $U_2 = 0.5$, 1.0, 1.5 and 2.0. For $U_2 = 0.5$ and 1.0, only fast ion-acoustic modes have real critical Mach numbers, $M_0 = (1.31$ and $-2.02)$ and (1.79 and -2.01), respectively, and they correspond to regular solitons. The slow ion-acoustic modes have complex conjugate roots, one is growing and the other is damped. This is due to the excitation of the ion beam instability of the slow ion-acoustic mode. All the four real critical Mach number, M_0, appear when $U_2 > U_{th} = 1.24$ and ion beam instability disappears. For $U_2 = 1.5$, the real critical Mach numbers occurring at $M_0 = 2.29$ and -2.0 (both fast ion-acoustic), 0.65 and 0.07 (both slow ion-acoustic). For $U_2 = 2.0$, the fast ion-acoustic modes occur at critical Mach number $M_0 = 2.78$ and -2.0, and slow ion-acoustic occur at $M_0 = 1.19$ and 0.032. Further, both type of fast ion-acoustic modes, and one slow ion-acoustic mode associated with the lowest positive critical $M_0 = 0.07$ and 0.032 are regular solitons, and the other slow acoustic modes are the new class of ion-acoustic solitons.

4. Summary and discussion

We have reported for the first time a new class of slow ion-acoustic solitons that occur below the critical Mach number in a three-component plasma system consisting of hot Max-wellian electrons and two counterstreaming ion beams. In contrast to the familiar fast and slow ion-acoustic solitons which exist in the Mach number range $M_0 < M < M_{\max}$, the new class of slow ion-acoustic solitons occur in the Mach number range $M_0 > M > M_{\min}$. We have discussed two special cases: 1. Equal ion beam densities and equal velocities of the counterstreaming ion beams, and 2. Unequal ion densities and unequal velocities of the counterstreaming ion beams. For both the cases, the new class of slow ion-acoustic solitons can occur only when the ion beam streaming speed exceeds some threshold value, U_{th}. For the parameters considered here, the threshold drift speed of the counterstreaming ion beams is found to be $U_{th} = 1.14$ for the case 1 (equal densities and velocities, section 2.1) and 1.24 for the case 2 (both densities and velocities being unequal, appendix) from the linear stability analysis. It is related to the disappearance of complex roots of slow ion-acoustic modes, and appearance of all four real roots of $F(M) = 0$ (section 3 and appendix). In other words, the new class of slow ion-acoustic solitons occur when the system is stable to ion beam instability. Although we have shown the existence of new class of slow ion-acoustic solitons under two special cases only, they are expected to occur over a wide range of ion beam densities and streaming velocities of the counterstreaming ion beams.

Ion beams have been observed in the polar cusp, auroral region and plasma sheet boundary layer of the Earth's magnetosphere [74–78]. Recently, from the analysis of high resolution data from the Magnetospheric Multiscale (MMS) mission in the Earth's magnetotail, Liu *et al* (2019) [79] have reported intense electrostatic solitary waves (ESWs) generated by cold ion beams in the reconnection jet region. Earlier, slow electrostatic solitary waves (ESWs) moving with speeds of the order of ion thermal speed or ion-acoustic speed have been observed at the reconnection sites [80, 81]. Later on, slow electrostatic solitary waves (ESWs) moving earthward with a speed close to 500 km s^{-1} in the plasma sheet boundary layer have been reported [82]. The new class of slow ion-acoustic solitons may be relevant in explaining the observations of these slow ESWs.

It is hoped that the discovery of new class of slow ion-acoustic solitons will generate enough interest in the plasma physics community for their verification by laboratory experiments, and also by computer simulations.

Acknowledgments

GSL thanks the Indian National Science Academy (INSA), New Delhi for the support under the INSA Honorary Scientist scheme.

Appendix. Unequal densities and velocities of the ion beams

Here we shall briefly discuss the linear stability for the case where both the densities and the velocities of the ion beams are unequal. For simplicity the temperatures of the ion beams are taken as equal.

A.1. Linear stability analysis

We consider a special case where $\sigma_1 = \sigma_2 = \sigma_p = 0.1$, $n_1^0 = 0.7$, $U_1 = -1.0$, $n_2^0 = 0.3$ and consider the stability of the system for different values of U_2, the velocity of ion beam 2. The dispersion relation computed from equation (6) for these parameters and for various values of U_2 is shown in Panels (a)–(d) of figure A1. In Panels (a) to (d) of figure A1, the curves 1 and 4 correspond to fast ion-acoustic modes and the curves 2 and 3 correspond to the slow ion-acoustic modes. The broken curves are for the real frequency, ω_r/ω_{pp}, and they follow the scale on left side of the panel. The solid curves are for the imaginary frequency, ω_i/ω_{pp}, and they follow the scale given on the right side of the panel. The positive or negative values of ω_i/ω_{pp} represent, respectively, the growth rate or the damping rate of the mode. Panel (a) for $U_2 = 0.5$ shows that the fast ion-acoustic modes (cf broken curves 1 and 4) have real frequencies. But, the slow ion-acoustic modes (curves 2 and 3) have complex conjugate frequencies. For one of the slow ion-acoustic mode ω_i/ω_{pp} is positive (cf solid curve 3), whereas for the other it is negative (cf solid curve 2). Therefore the system is unstable to ion beam instability. In Panel (b), which is for $U_2 = 1.0$, the fast ion-acoustic modes (broken curves 1 and 4) have real roots, whereas the slow ion-acoustic mode 2 is damped and slow mode 3 is unstable for $0 < k\lambda_{de} < 0.58$ (cf solid curves 2 and 3). For $k\lambda_{de} > 0.58$, slow ion-acoustic modes have real frequencies (cf broken curves 2 and 3). Hence, the system is unstable to ion beam instability for $0 < k\lambda_{de} < 0.58$, and stable for $k\lambda_{de} > 0.58$. Panel (c) is for $U_2 = 1.5$, both the fast ion-acoustic modes (broken curves 1 and 4) and slow ion-acoustic modes (broken curves 2 and 3) have real frequencies only, and the system is stable against ion beam instability. Panel (d), $U_2 = 2.0$, again all modes have distinct real frequencies (broken curves 1–4) showing a stable plasma system. It is interesting to note that one of the slow ion-acoustic mode (curve 3) in Panels (c) and (d) has initially positive values for $0 < k\lambda_{de} < 0.45$, and then negative values for $k\lambda_{de} > 0.45$. For the parameters considered here, we find numerically that the ion beam instability exists for U_2 values in a range of $0.13 \leqslant U_2 < 1.24$ (not shown). Considering different values of n_1^0, n_2^0, and U_1 will change the unstable U_2 range.

In contrast to figure 1, where both the fast and slow ion-acoustic modes have exactly equal and opposite real frequencies for the parallel and anti-parallel modes, here the real frequencies do not have exactly equal values in magnitude and sign. This is because the unequal densities as well as unequal beam velocities break the symmetry in the system. Although we have not shown here, ion beams having unequal temperatures are also found to produce similar effects.

A.2. Critical Mach numbers for the case of Unequal densities and ion beam velocities

In this section we shall show that the critical Mach numbers M_0, found from $F(M_0) = 0$. where $F(M)$ is given by equation (13), for the case of ion beams having unequal densities and unequal streaming velocities have, in general, different values (in magnitude and sign) from each other for both fast and slow ion-acoustic mode. The new class of slow

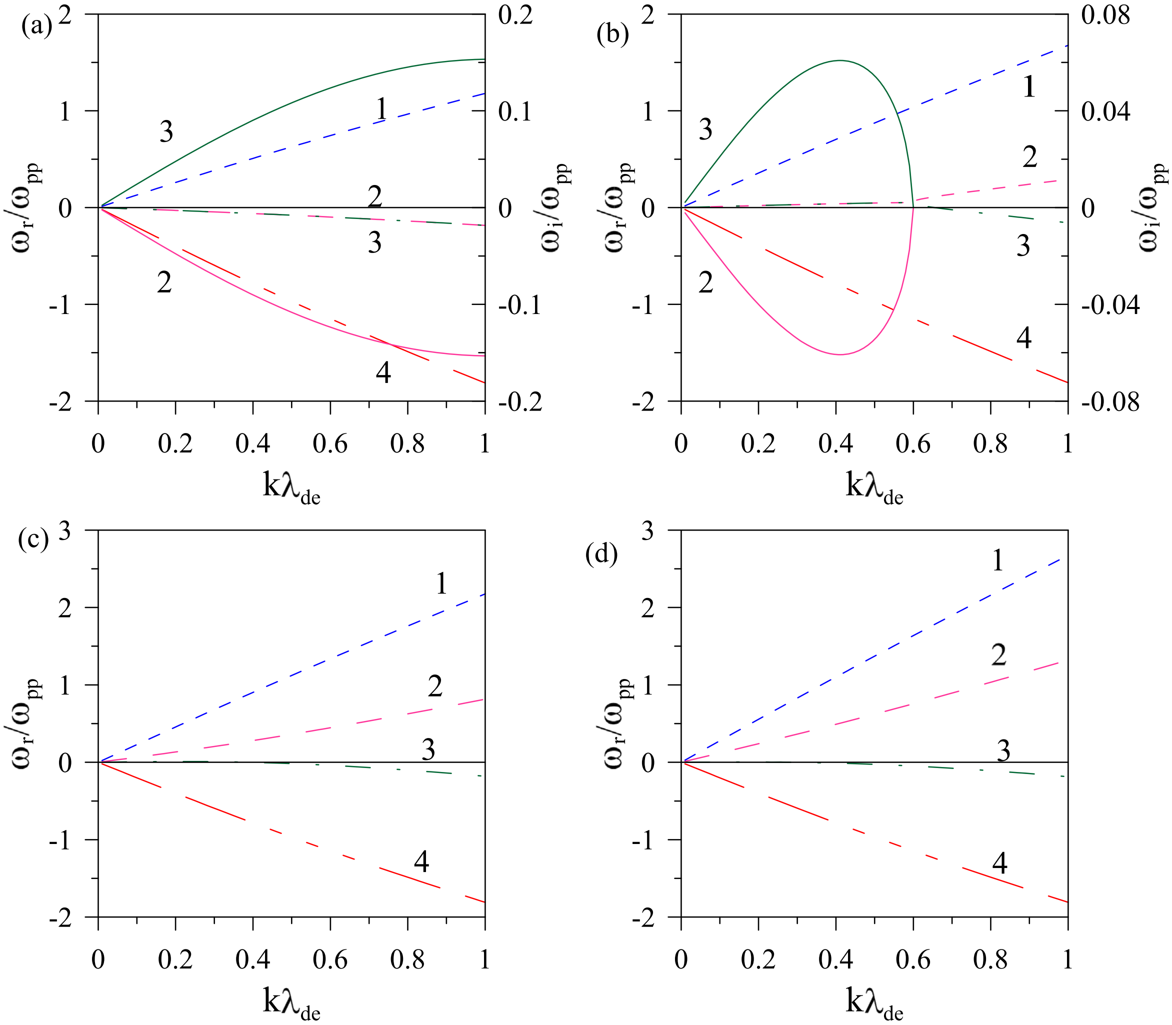

Figure A1. Dispersion relation for the ion-acoustic waves showing the normalized frequency ω/ω_{pp} versus normalized wave number, $k\lambda_{de}$ for the case of unequal beam densities and unequal beam velocities but equal ion beam temperatures. The normalized parameters are $n_1^0 = 0.7$, $U_1 = -1.0$, $n_2^0 = 0.3$ and $\sigma_1 = \sigma_2 = \sigma_p = 0.1$. In Panels (a) to (d), the curves 1 and 4 correspond to fast ion-acoustic modes and the curves 2 and 3 correspond to the slow ion-acoustic modes. The broken curves are for the real frequency, ω_r/ω_{pp}, and they follow the scale on left side of the panel. The solid curves are for the imaginary frequency, ω_i/ω_{pp}, and they follow the scale given on the right side of the panel. The positive or negative values of ω_i/ω_{pp} represent, respectively, the growth rate or the damping rate of the mode. Panel (a) is for $U_2 = 0.5$; the fast ion-acoustic modes (cf broken curves 1 and 4) have real frequencies. The slow ion-acoustic modes (curves 2 and 3) have complex conjugate frequencies. Panel (b) is for $U_2 = 1.0$, the fast ion-acoustic modes (broken curves 1 and 4) have real roots, whereas the slow ion-acoustic mode 2 is damped and slow mode 3 is unstable for $0 < k\lambda_{de} < 0.58$ (cf solid curves 2 and 3). For $k\lambda_{de} > 0.58$, slow ion-acoustic modes have real frequencies (cf broken curves 2 and 3). Panel (c) is for $U_2 = 1.5$, both the fast ion-acoustic modes (broken curves 1 and 4) and slow ion-acoustic modes (broken curves 2 and 3) have real frequencies only, and the system is stable. Panel (d), $U_2 = 2.0$, all modes have distinct real frequencies (broken curves 1-4), and the system is stable against the ion beam instability.

ion-acoustic solitons can exist in the parametric regime where the system is stable to ion beam instability.

Figure A2 shows variations of $F(M)$, the second derivative of the Sagdeev pseudopotential $S(\phi, M)$ at $\phi = 0$, versus the Mach number M for the case of unequal beam densities and beam velocities, but equal ion beam temperatures, for the same parameters as for figure A1. From Panel (a) of figure A2 which is for $U_2 = 0.5$, it is seen that two critical Mach numbers (fast ion-acoustic) occur at $M_0 = 1.31$ (R1) and -2.02 (R4). Other two roots R2 and R3 corresponding to the slow ion-acoustic modes are complex conjugate, where one mode is growing, the other is damped. This happens due to the excitation of slow ion-acoustic mode instability by the ion beams. Further, it is seen that for the real roots R1 and R4, the $F(M)$ curves go below the M-axis when M exceeds M_0, and the soliton condition $F(M) < 0$ is satisfied. Panel (b) of figure A2 is for $U_2 = 1.0$, here also only two critical Mach numbers (fast ion-acoustic) are real occurring at $M_0 = 1.79$ (R1) and -2.01 (R4), the other two roots corresponding to slow ion-acoustic mode are complex conjugate. Therefore, the system is unstable to ion beam instability. In this case also for the roots R1 and R4, the $F(M)$ curves go below the M-axis when M exceeds M_0, and the soliton condition $F(M) < 0$ is satisfied. It is seen from Panel (c) for $U_2 = 1.5$, that there are four real critical Mach numbers occurring at $M_0 = 2.29$ (R1) and -2.0 (R4) (both fast ion-acoustic), 0.65 (R2) and

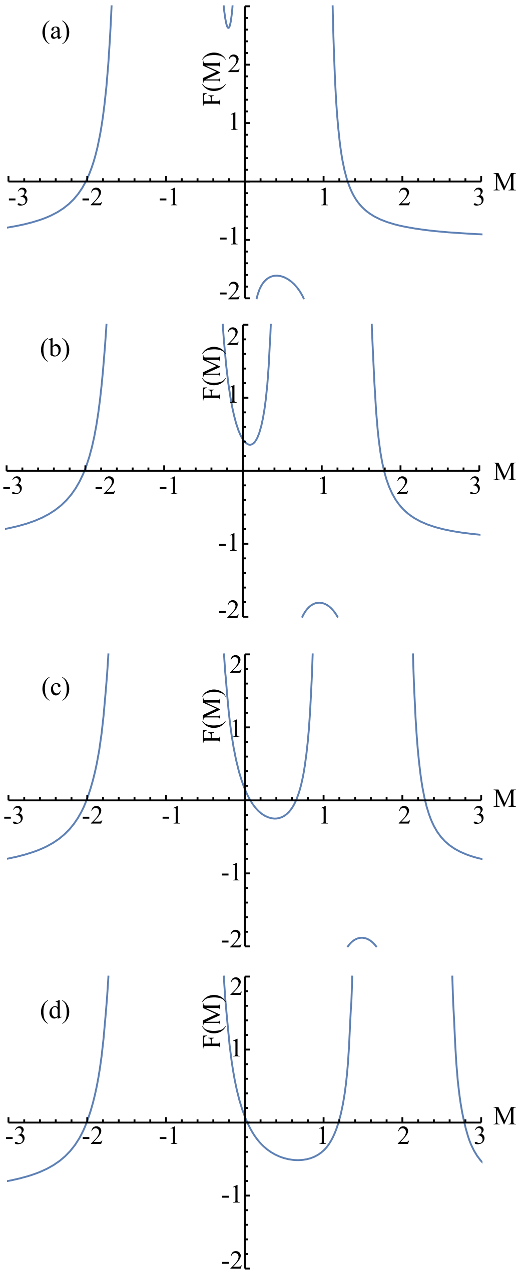

Figure A2. Variation of $F(M)$, the second derivative of the Sagdeev pseudopotential $S(\phi, M)$ at $\phi = 0$, *versus* the Mach number M for the case of unequal beam densities and unequal beam velocities but equal ion beam temperatures. The normalized parameters are $\sigma_1 = \sigma_2 = \sigma_p = 0.1$, $n_1^0 = 0.7$, $n_2^0 = 0.3$, $U_1 = -1.0$. In Panel (a), $U_2 = 0.5$, two critical Mach numbers (fast ion-acoustic) occur at $M_0 = 1.31$ and -2.02, and the other two roots (slow ion-acoustic) are complex conjugate. Panel (b)is for $U_2 = 1.0$, only two critical Mach numbers (fast ion-acoustic) are real occurring at $M_0 = 1.79$ and -2.01, the other two roots corresponding to slow ion-acoustic mode are complex conjugate. Panel (c) is for $U_2 = 1.5$, there are four real critical Mach numbers occurring at $M_0 = 2.29$ and -2.0 (both fast ion-acoustic), 0.65 and 0.07 (both slow ion-acoustic). Panel (d), $U_2 = 2.0$, all four roots are real. The fast ion-acoustic modes occur at critical Mach number $M_0 = 2.78$ and -2.0, and slow ion-acoustic occur at $M_0 = 1.19$ and 0.032.

0.07 (R3) (both slow ion-acoustic). This shows that the system is stable which is consistent with the linear analysis shown in figure A1. Panel (d) of figure A2 is for $U_2 = 2.0$, here all four roots are real. The fast ion-acoustic modes occur at critical Mach number $M_0 = 2.78$ (R1) and -2.0 (R4), and slow ion-acoustic occur at $M_0 = 1.19$ (R2) and 0.032 (R3).

It is worth point out that all four real critical Mach number, M_0, appear when $U_2 > U_{th} = 1.24$ which is consistent with the linear stability analysis discussed above. It is interesting to note that in both the Panels (c) and (d) of figure A2, for the real roots R1, R3 and R4, the soliton condition $F(M) < 0$ is satisfied for $M > M_0$. However, for the root R2 in Panels (c) and (d), it is seen that the the soliton condition $F(M) < 0$ is satisfied when $M < M_0$. Therefore, the new class of slow ion-acoustic solitons can exist in the parametric regime where the system is stable against ion beam instability.

ORCID iDs

G S Lakhina https://orcid.org/0000-0002-8956-486X
S V Singh https://orcid.org/0000-0003-2758-7713

References

[1] Sagdeev R Z 1966 *Rev Plasma Phys, Consultant Bureu, New York* **4** 23–91
[2] Washimi H and Taniuti T 1966 *Phys. Rev. Lett.* **17** 996–8
[3] Tran M Q 1979 *Phys. Scripta* **20** 317–27
[4] Buti B 1980 *Phys. Lett.* A **76** 251–4
[5] Chanteur G and Raadu M 1987 *Phys. Fluids* **30** 2708–19
[6] Baboolal S, Bharuthram R and Hellberg M A 1990 *J. Plasma Physics* **44** 1–23
[7] Reddy R V and Lakhina G S 1991 *Planet. Space Sci.* **39** 1343–50
[8] Reddy R V, Lakhina G and Verheest F 1992 *Planet. Space Sci.* **40** 1055–62
[9] Ghosh S S, Ghosh K K and Iyengar A N S 1996 *Phys. Plasmas* **3** 3939–46
[10] Ghosh S S and Iyengar A N S 1997 *Phys. Plasmas* **4** 3204–10
[11] Berthomier M, Pottelette R and Malingre M 1998 *J. Geophys. Res.* **103** 4261–70
[12] Ghosh S S and Lakhina G S 2004 *Nonlinear Proc. Geoph.* **11** 219–28
[13] Hellberg M A and Verheest F 2008 *Phys. Plasmas* **15** 062307
[14] Lakhina G S, Kakad A P, Singh S V and Verheest F 2008 *Phys. Plasmas* **15** 062903
[15] Lakhina G S, Singh S V, Kakad A P, Verheest F and Bharuthram R 2008 *Nonlinear Processes Geophys.* **15** 903–13
[16] Lakhina G S, Singh S V and Kakad A P 2011 *Adv. Space Res.* **47** 1558–67
[17] Lakhina G S, Singh S V, Kakad A P and Pickett J S 2011 *J. Geophys. Res.* **116** A10218
[18] Maharaj S K, Bharuthram R, Singh S V and Lakhina G S 2012 *Phys. Plasmas* **19** 072320
[19] Singh S V, Devanandhan S, Lakhina G S and Bharuthram R 2013 *Phys. Plasmas* **20** 012306
[20] Rufai O R, Bharuthram R, Singh S V and Lakhina G S 2012 *Phys. Plasmas* **19** 122308
[21] Rufai O R, Bharuthram R, Singh S V and Lakhina G S 2014 *Commun. Nonl. Sci. Numer. Simulat.* **21** 1338–46
[22] Rufai O R, Bharuthram R, Singh S V and Lakhina G S 2014 *Phys. Plasmas* **21** 082304
[23] Singh S V and Lakhina G S 2015 *Commun. Nonl. Sci. Numer. Simulat.* **23** 274–81

[24] Maharaj S K, Bharuthram R, Singh S V and Lakhina G S 2015 *Phys. Plasmas* **22** 032313
[25] Rufai O R, Bharuthram R, Singh S V and Lakhina G S 2015 *Phys. Plasmas* **22** 102305
[26] Rufai O R, Bharuthram R, Singh S V and Lakhina G S 2016 *Adv. Space Res.* **57** 813–20
[27] Rufai O R, Bharuthram R, Singh S V and Lakhina G S 2016 *Phys. Plasmas* **23** 032309
[28] Kakad A, Kakad B, Anekallu C, Lakhina G, Omura Y and Fazakerley A 2016 *J. Geophys. Res.* **121** 4452–65
[29] Mahmood S and Ur-Rehman H 2013 *J. Phys. Soc. Japan* **82** 074501
[30] Lakhina G S, Singh S V and Kakad A P 2014 *Phys. Plasmas* **21** 062311
[31] Ur-Rehman H, Mahmood S and ur Rehman A 2014 *Phys. Scripta* **89** 105605
[32] Temerin M, Cerny K, Lotko W and Mozer F S 1982 *Phys. Rev. Lett.* **48** 1175–9
[33] Boström R, Gustafsson G, Holback B, Holmgren G, Koskinen H and Kintner P 1988 *Phys. Rev. Lett.* **61** 82–5
[34] Koskinen H E J, Lundin R and Holback B 1990 *J. Geophys. Res.* **95** 5921–9
[35] Matsumoto H, Kojima H, Miyatake T, Omura Y, Okada M, Nagano I and Tsutsui M 1994 *Geophys. Res. Lett.* **21** 2915–8
[36] Franz J R, Kintner P M and Pickett J S 1998 *Geophys. Res. Lett.* **25** 1277–80
[37] Tsurutani B T, Arballo J K, Lakhina G S, Ho C M, Buti B, Pickett J S and Gurnett D A 1998 *Geophys. Res. Lett.* **25** 4117–20
[38] Pickett J S *et al* 1999 *Adv. Space Res.* **24** 23–33
[39] Pickett J S, Menietti J D, Dowell J H, Gurnett D A and Scudder J D 1999 *Nonlin. Process. Geophys* **6** 195–204
[40] Ergun R E *et al* 1998 *Geophys. Res. Lett.* **25** 2041–4
[41] Ergun R E, Carlson C W, McFadden J P, Mozer F S, Muschietti L, Roth I and Strangeway R J 1998 *Phys. Rev. Lett.* **81** 826–9
[42] Pickett J S, Chen L J, Kahler S W, Santolík O, Gurnett D A, Tsurutani B T and Balogh A 2004 *Ann. Geophys.* **22** 2515–23
[43] Mangeney A, Salem C, Lacombe C, Bougeret J L, Perche C, Manning R, Kellogg P J, Goetz K, Monson S J and Bosqued J M 1999 *Ann. Geophys.* **17** 307–20
[44] Saini N S, Kourakis I and Hellberg M A 2009 *Phy. Plasmas* **16** 062903
[45] Saini N S and Kourakis I 2010 *Plasma Phys. Controlled Fusion* **52** 075009
[46] Verheest F and Hellberg M A 2010 *Phys. Plasmas* **17** 102312
[47] Baluku T K and Hellberg M A 2012 *Phys. Plasmas* **19** 012106
[48] Lakhina G S and Singh S V 2015 *Solar Phys.* **290** 3033–49
[49] Rubia R, Singh S V and Lakhina G S 2016 *Phys. Plasmas* **23** 062902
[50] Lakhina G S and Singh S 2017 Chapter 9—solitary waves in plasmas described by kappa distributions *Kappa Distributions: Theory and Applications in Plasmas* ed G Livadiotis (Amsterdam: Elsevier) pp 399–418
[51] Rubia R, Singh S V and Lakhina G S 2017 *J. Geophys. Res.* **122** 9134–47
[52] Rubia R, Singh S V and Lakhina G S 2018 *Phys. Plasmas* **25** 032302
[53] Dubinov A E and Kolotkov D Y 2012 *Plasma Phys. Rep.* **38** 909–12
[54] Dubinov A E and Kolotkov D Y 2012 *IEEE Trans. Plasma Sci.* **40** 1429–33
[55] Verheest F, Hellberg M A and Kourakis I 2013 *Phys. Plasmas* **20** 012302
[56] Verheest F, Hellberg M A and Kourakis I 2013 *Phys. Plasmas* **20** 082309
[57] Maharaj S K, Bharuthram R, Singh S V and Lakhina G S 2013 *Phys. Plasmas* **20** 083705
[58] Verheest F, Lakhina G S and Hellberg M A 2014 *Phys. Plasmas* **21** 062303
[59] Ikezi H, Taylor R J and Baker D R 1970 *Phys. Rev. Lett.* **25** 11–4
[60] Ikezi H 1973 *Phys. Fluids* **16** 1668
[61] Nakamura Y 1982 *IEEE Trans. Plasma Sci* **PS-10** 180–95
[62] Lonngren K E 1998 *Opt. Quantum Electron.* **30** 615–30
[63] Georgin M P, Jorns B A and Gallimore A D 2018 *II Space Propulsion Conf., Sevilla, Spain* SPC18-403, 1–2
[64] Kakad A, Omura Y and Kakad B 2013 *Phys. Plasmas* **20** 062103
[65] Kakad B, Kakad A and Omura Y 2014 *J. Geophy. Res.: Space Physics* **119** 5589–99
[66] Kakad A, Kakad B and Omura Y 2017 *Phys. Plasmas* **24** 060704
[67] Lotekar A, Kakad A and Kakad B 2016 *Phys. Plasmas* **23** 102108
[68] Lotekar A, Kakad A and Kakad B 2017 *Phys. Plasmas* **24** 102127
[69] Crumley J P, Cattell C A, Lysak R L and Dombeck J P 2001 *J. Geophys. Res.: Space Physics* **106** 6007–15
[70] Malkov M A, Sagdeev R Z, Dudnikova G I, Liseykina T V, Diamond P H, Papadopoulos K, Liu C S and Su J J 2016 *Phys. Plasmas* **23** 043105
[71] Lakhina G S, Singh S V, Rubia R and Sreeraj T 2018 *Phys. Plasmas* **25** 080501
[72] Sreeraj T, Singh S V and Lakhina G S 2016 *Phys. Plasmas* **23** 082901
[73] Vedenov A A, Velikhov E P and Sagdeev R Z 1961 *Soviet Physics Uspekhi* **4** 332–69
[74] Gurnett D A and Frank L A 1978 *J. Geophys. Res.* **83** 1447–62
[75] D´Angelo N 1977 *Rev. Geophys. Space Phys.* **15** 299–307
[76] Parks G K *et al* 1984 *J. Geophys. Res.* **89** 8885–906
[77] Takada T, Seki K, Hirahara M, Fujimoto M, Saito Y, Hayakawa H and Mukai T 2005 *J. Geophys. Res.* **110** A02204
[78] Grison B, Sahraoui F, Lavraud B, Chust T, Cornilleau-Wehrlin N, Rème H, Balogh A and André M 2005 *Ann. Geophys.* **23** 3699–713
[79] Liu C M, Vaivads A, Graham D B, Khotyaintsev Y V, Fu H S, Johlander A, André M and Giles B L 2019 *Geophys. Res. Lett.* **46** 1–9
[80] Khotyaintsev Y V, Vaivads A, André M, Fujimoto M, Retino A and Owen C J 2010 *Phys. Rev. Lett.* **105** 165002
[81] Graham D B, Khotyaintsev Y V, Vaivads A and André M 2015 *Geophys. Res. Lett.* **42** 215–24
[82] Norgren C, André M, Vaivads A and Khotyaintsev Y V 2015 *Geophys. Res. Lett.* **42** 1654–61